Optics Letters

Kerr nonlinearity and dispersion characterization of core-pumped thulium-doped fiber at 2 μm

Svyatoslav Kharitonov,* Adrien Billat, and Camille-Sophie Brès

Ecole Polytechnique Fédérale de Lausanne (EPFL), Photonic Systems Laboratory, CH-1015 Lausanne, Switzerland
**Corresponding author: svyatoslav.kharitonov@epfl.ch*

Received 12 May 2016; revised 11 June 2016; accepted 12 June 2016; posted 13 June 2016 (Doc. ID 265036); published 5 July 2016

A nonlinear coefficient of 3.6–4.1 W^{-1} km^{-1} and group velocity dispersion of −20 ps^2/km of a commercial core-pumped thulium-doped fiber have been evaluated using degenerate four-wave mixing at 2 μm. The anomalous dispersion behavior of the fiber has been confirmed by linear measurements with an all-fiber Mach–Zehnder interferometer (MZI). Additionally, no pump-induced dispersion changes due to excitation of Tm^{3+} cations have been detected. These characteristics make these fibers attractive for pulsed fiber laser applications. A nonlinear-polarization rotation mode-locked laser involving nonlinear polarization evolution directly in the doped fiber is demonstrated.

OCIS codes: (060.2270) Fiber characterization; (260.2030) Dispersion; (060.2390) Fiber optics, infrared; (190.4380) Nonlinear optics, four-wave mixing; (060.3510) Lasers, fiber.

http://dx.doi.org/10.1364/OL.41.003173

Thulium-doped fiber (TDF) lasers operating in the 2 μm spectral range have recently attracted significant interest for various applications, covering spectroscopy and atmospheric CO_2 monitoring, material and biological tissues processing, and telecommunications [1–5]. TDFs and a whole range of fiber optics components designed to operate around 2 μm have emerged during the past years and are now widely available, simplifying the implementation of lasers and amplifiers.

Thulium-doped fibers can be purchased off the shelf, but some of their characteristics, namely, dispersion and nonlinearity, are rarely studied despite their impact on many applications. 2 μm pulsed lasers have undergone tremendous advances over the past few years, with continuous performance improvements in terms of pulse duration and peak and average powers [4]. Dispersion management of the fiber cavity enables the generation of soliton or similariton (parabolic) pulses [6] when a saturable absorber is included. Solid-state saturable absorbers (SESAMs [6], graphene [7]), or Kerr-nonlinear switching elements (nonlinear optical/amplifying loop mirrors [8]), or combinations of both of them [9], were used to modulate cavity losses. Particularly, nonlinear polarization rotation (NPR) is a straightforward and easy-to-implement effect to lock the cavity [10]. In any case, the dispersion and nonlinearity of the various fibers used in the cavity have a direct impact on the performance of the laser. Even though the realization of powerful lasers (over a few watts) requires the use of double-clad fibers for pump coupling matters, the 2 μm mode propagates mostly in the core, the diameter of which can be compared to that of an SMF-28 (e.g., 10 μm for Nufern SM-TDF-10P/130-HE). It can therefore experience significant nonlinear effects due to the high field intensity in the doped fiber over a cavity round trip. TDF amplifiers have also become an active topic of research in the telecommunication field since the demonstration of long haul transmission at 2 μm in hollow-core fibers [5]. Due to the impressive bandwidth of such amplifiers (roughly from 1.8 to 2.1 μm [11]), this spectral band is seen as a potential solution to overcome the capacity limit of fiber networks. It is therefore crucial to study the nonlinear and dispersive properties of single core TDF, such as the standard TmDF200 by OFS (OFS Fitel Denmark ApS).

As TmDF200 fiber features a small core diameter (evaluated at 3.8 μm) and a high index contrast between the core and the cladding (numerical aperture NA = 0.26), interesting behavior in terms of dispersion and nonlinearity can be expected, and an experimental investigation of their chromatic dispersion and Kerr coefficient at 2 μm was performed. The experimental study described throughout this Letter is composed of two parts. First, degenerate four-wave mixing (FWM) among a relatively powerful subwatt level continuous-wave (CW) parametric pump, a signal, and an idler, the three of them located around 2000 nm, is investigated to quantify the nonlinear coefficient, the linear attenuation, and the dispersion of the TDF at the pump wavelength. Second, a linear measurement of TDF dispersion is performed using an all-fiber Mach–Zehnder interferometer (MZI) setup seeded with a wideband supercontinuum in order to confirm the sign and magnitude of the retrieved 2 μm dispersion. Moreover, a preliminary study of the impact of population inversion on the dispersion is also done using the MZI. The experiments suggest that the TDF exhibits nonlinearities 5 times larger than single-mode fiber (SMF) and a strong anomalous dispersion. The former is verified through a proof-of-concept demonstration of mode locking based on nonlinear polarization rotation solely in TDF.

The setup for FWM characterization is shown in Fig. 1(a). Two custom-made polarized CW fiber lasers are used to generate the pump and the signal (degree of polarization better

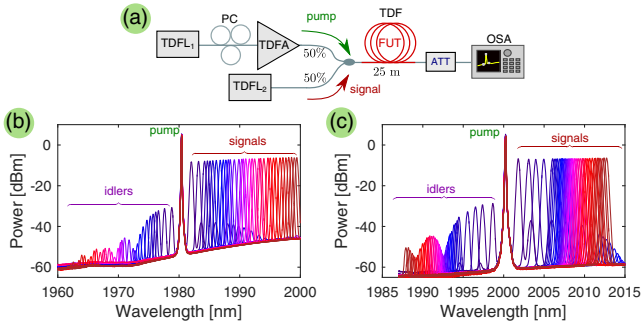

Fig. 1. (a) Experimental setup for the FWM characterization of the FUT: TDFL, thulium-doped fiber lasers; TDFA, thulium-doped fiber amplifier; PC, polarization controller; OSA, optical spectrum analyzer; ATT, attenuator. Superimposed spectra at the FUT output for a range of pump-signal detuning, and pumping wavelengths of (b) 1980.4 and (c) 2000.2 nm. OSA resolution: 0.05 nm.

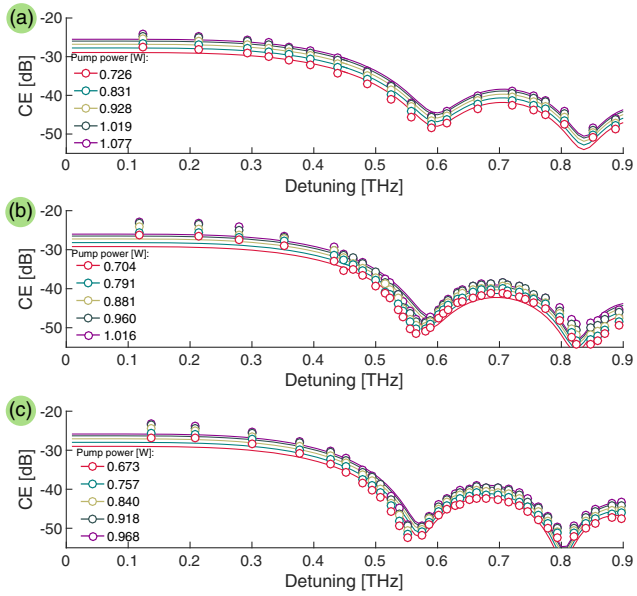

Fig. 2. CE spectra for a pump wavelength of (a) 1980, (b) 2000, and (c) 2008 nm, and for five pump powers. Circles, experimental data; solid lines, corresponding optimal fits, calculated using Eq. (1).

than 18 dB). Both consist of a unidirectional ring cavity [12,13], in which the wavelength-selective element is either a fiber Bragg grating (FBG) in conjunction with a circulator (for the pump) or a tunable bandpass filter (BPF) (for the signal). The pump laser is first amplified in a commercial 2 μm booster before being combined with the signal laser via a 50/50 coupler. Both waves are then directed toward the 25 m long fiber under test (FUT), where FWM along the propagation gives rise to an idler wave. The conversion efficiency (CE) is defined as the idler power at the fiber output divided by signal power at the input. The BPF in the signal laser cavity allows for its wavelength to be tuned away from the pump, and to reconstruct the CE spectrum as a function of pump-signal frequency detuning. Typical FWM spectra, recorded with an optical spectrum analyzer (OSA) after the FUT, are displayed in Figs. 1(b) and 1(c) for parametric pumping wavelengths of 1980 and 2000 nm, respectively. On the long wavelength side of the pump, we observed strong spontaneous emission from the booster as well as from the FUT. The later is due to absorption around 2 μm originating from the $^3F_4 \rightarrow {}^3H_6$ transition. The signal was therefore deliberately positioned on the Stokes side of the pump such that idlers are created on the anti-Stokes side, where the reduced amplified spontaneous emission (ASE) enables the detection of low magnitude idlers.

Before the FWM experiments, the signal power was recorded at the FUT input over the whole wavelength range for the CE reconstruction. In the presence of propagation losses, the signal-to-idler parametric conversion in the degenerate FWM case can be described by [14]:

$$G = \left|\frac{e^{-\alpha L}\pi\gamma P}{\alpha \sin \pi\gamma}\right|^2 |J_\nu(Z(0))J_{-\nu}(Z) - J_{-\nu}(Z(0))J_\nu(Z)|^2, \quad (1)$$

where L is the fiber length, γ is the nonlinear coefficient, α is the fiber attenuation, $J_\nu(Z)$ is the Bessel function of the first kind and complex order $\nu = 1 + i\Delta\beta_L/\alpha$, $Z(L) = 2\alpha^{-1}[\Delta\beta_L\gamma P \exp(-\alpha L)]^{1/2}$, $\Delta\beta_L = \beta_2(\Delta\omega)^2$ is the linear phase mismatch, and $\Delta\omega$ is the angular frequency pump-signal detuning. This model assumes that the attenuation coefficients experienced by the three waves are equal. In an active medium with spectrally sharp absorption or emission cross sections, such an assumption can be incorrect. However, it yields an accurate fitting in our configuration when some precautions are taken, as will be discussed below. The difference between the experimental CE data points and its theoretical spectrum [Eq. (1)] is then minimized using the MATLAB optimization toolbox. The fitting parameters are γ, β_2, and α. During the experimental data acquisition, the pump power was varied from 0.7 to 1.1 W, and the fittings of the CE spectra are expected to yield the same parameter set for all input powers. The acquisition was performed for three pumping wavelengths: 1980, 2000, and 2008 nm. The CE spectra, as functions of the pump-signal frequency detuning, are shown in Fig. 2, with their respective optimal fittings in all cases. Table 1 summarizes the parameters retrieved from the curves.

Discrepancies between experimental and theoretical fits can be observed for small (below 0.4 THz) detuning in Fig. 2. They originate from the nonuniform absorption in the TDF, not taken into account in the CE model. The absorption cross section linked to the $^3F_4 \rightarrow {}^3H_6$ transition smoothly decreases toward zero in this band [15]. In our configuration, this results in an idler undergoing stronger linear attenuation than both the pump and the signal when the Tm^{3+} population is not inverted. Consequently, the higher the detuning, the less accurate the model is in describing the CE, and it is impossible to obtain a perfect fitting both for small and large frequency detuning with the same parameter set. The fitting procedure is therefore

Table 1. Summary of Retrieved Parameters (Mean and Standard Deviation Values)

λ_p(nm)	β_2(ps^2 · km^{-1})	γ(W^{-1} · km^{-1})	α(dB · m^{-1})
1980	−18.41 ± 0.38	3.87 ± 0.29	0.12 ± 0.02
2000	−18.94 ± 0.11	3.39 ± 0.43	0.10 ± 0.04
2008	−19.91 ± 0.38	3.21 ± 0.49	0.07 ± 0.03

Table 2. Final Extracted Parameters (Mean and Standard Deviation Values)

λ_p(nm)	β_2(ps^2 · km^{-1})	γ(W^{-1} · km^{-1})	α(dB · m^{-1})
1980	−18.74 ± 0.39	4.09 ± 0.41	0.12 ± 0.02
2000	−19.81 ± 0.14	3.80 ± 0.15	0.07 ± 0.03
2008	−20.49 ± 0.36	3.57 ± 0.33	0.06 ± 0.01

refined by focusing on characteristic regions of the CE spectrum. First, for relatively high dispersion (tens of ps^2/km, as is the case here), the spectral position of the dips and lobes is defined almost exclusively by the β_2 coefficient. Also, the fiber absorption coefficient α broadens the spectral dips and reduces their depth. By applying the fitting algorithm to CE spectra around the first dip, one can estimate β_2 and α. The remaining parameter γ is then extracted by focusing on the CE in the proximity of the pump (small detuning) that is the most correctly described by the analytical formula. The refined parameters extracted at each pump wavelength are presented in Table 2.

These results show that the FUT features a relatively strong nonlinear coefficient, in the range 3.6–4.1 W^{-1} km^{-1}, that allows FWM to be detected in spite of a strong chromatic dispersion, the 1 THz pump-signal detuning, and pump powers as low as 0.7 W. Keeping in mind that γ scales with pump frequency, the TDF is 4–5 times more nonlinear than a standard SMF-28 at 2 μm (0.9 W^{-1} km^{-1}). The TmDF200 fiber characteristics (dispersion, mode effective area) were calculated assuming cladding refractive index of pure SiO_2, $n_{clad} = n_{SiO_2}$, and core refractive index $n_{core} = \sqrt{n_{SiO_2}^2 + NA^2}$. The NA value is taken from fiber specifications. The core diameter of 3.8 μm is optimized to match a mode field diameter of 5 μm at 1700 nm, provided by the manufacturer. From these values, a nonlinear refractive index n_2 of 3.25–3.55 10^{-20} m^2 W^{-1} is evaluated. Nonetheless, it should be noted that for such high dispersion, the CE spectrum virtually does not change if the dispersion coefficient sign is flipped. Therefore, linear interferometric measurements are performed to verify the anomalous dispersion, and to cross check the quality of CE fitting.

Linear dispersion measurements are performed with an all-fiber MZI [Fig. 3(a)]. The FUT is placed in one arm, while the second arm includes a tunable optical delay line (ODL) and a section of balance fiber (e.g., SMF-28e). The interferometric measurement technique relies on the tracking of a broad central fringe position [16]. A custom pulsed supercontinuum source covering entirely the 1.4–2.15 μm range is used as an input source. The FUT arm of the MZI also includes a 1.6–2 μm wavelength-division multiplexer to enable the independent excitation of the $^3F_4 \rightarrow {}^3H_6$ transition using a 1.6 μm pump. A variable optical attenuator (VOA) is used to equalize the powers in both arms once the Tm^{3+} pump is applied. The ODL time delay τ is swept to move the central fringe wavelength over the bandwidth of the supercontinuum source (SC) [Fig. 3(b)].

Dispersion evaluation results are summarized in Fig. 3(c) and compared with simulated data. The interferometric measurements confirm the anomalous dispersion behavior of the TDF fiber, while the FWM-extracted data is in good agreement with theoretical calculations. A small shift between MZI-measured and simulated curves can be caused by a

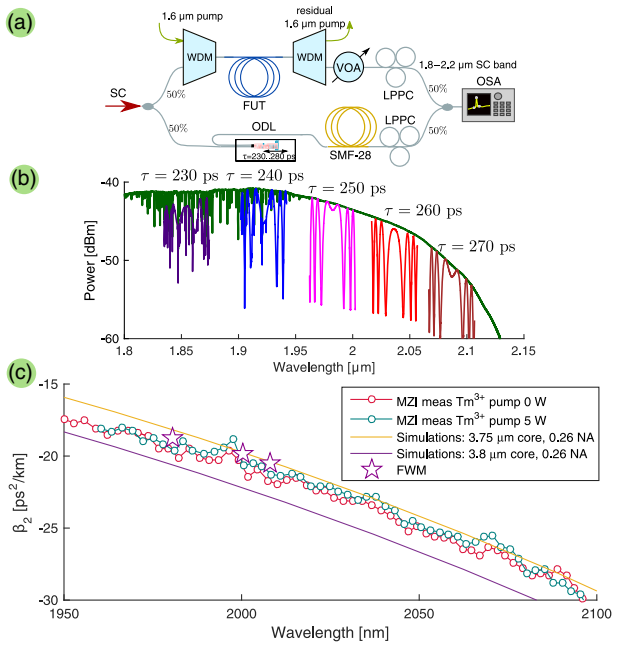

Fig. 3. (a) MZI experimental setup: SC, supercontinuum source; WDM, wavelength-division multiplexer; VOA, variable optical attenuator; ODL, optical delay line; LPPC, large-paddle polarization controller. (b) SC spectrum, superimposed with interferograms for selected values of τ. (c) Dispersion characterization comparison between FWM-extracted data, and MZI-measured data for the case of nonexcited and excited $^3F_4 \rightarrow {}^3H_6$ Tm^{3+} transition (0 and 5 W 1.6 μm pump, respectively).

deviation of zero-dispersion wavelength of the SMF-28e fiber from its mean value. Therefore, the FWM experiment offers higher precision of β_2 determination, as no referencing is needed. The other remarkable point is that the MZI experiment does not reveal any significant resonant changes of TDF dispersion between the pumped and unpumped cases [5 and 0 W of Tm^{3+} pump at 1600 nm, respectively; Fig. 3(a)]. The MZI-based dispersion measurement setup was also tested with an erbium-doped fiber (EDF), and a characteristic resonant dispersion flipping was observed under 980 nm pumping (similar to a previous report [17]). The latter experiment proves the setup capability to detect pump-induced dispersion changes.

These initial results not only provide a quantitative characterization of the fiber but also represent interesting information that can be further leveraged. In particular, such TDF with relatively large γ at 2 μm can be exploited as a component for Kerr-nonlinear switching element in mode-locked fiber lasers (MLL). NPR-based laser configurations reported so far include considerable lengths (up to 100 m) of additional fiber (SMF-28, SM2000) to ensure proper nonlinear polarization evolution within the cavity, which decreases the pulse repetition rate. Within this Letter, we report NPR MLL, where nonlinear polarization evolution occurs mainly directly within the TDF. The experimental setup is shown in Fig. 4(a). The laser consists of 11.5 m of previously characterized TDF, bidirectionally core pumped with a 1600 nm pump obtained from an amplified tunable laser source (TLS), a polarization controller (PC), and a polarization beam splitter (PBS), which acts as saturable

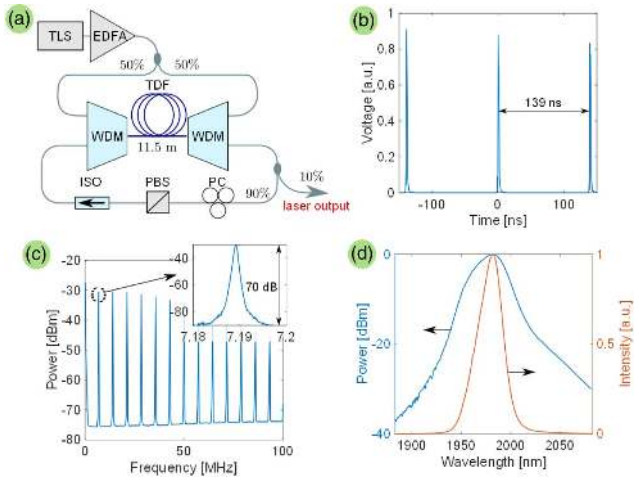

Fig. 4. (a) Layout of NPR-based thulium-doped mode-locked fiber laser. Laser characterization results: (b) temporal waveform; (c) electrical spectrum [resolution bandwidth (RBW) of 1 MHz], inset shows zoom of the first frequency line with electrical signal-to-noise ratio of 70 dB (RBW of 100 kHz); (d) optical spectrum, 1 nm resolution.

absorber on the pulsed signal with power-dependent polarization. The isolator (ISO) ensures unidirectional lasing, and the laser output is obtained at a 10% power coupler. The total pump power is 3 W.

The laser output is analyzed using optical and electrical spectrum analyzers (ESAs), and a 500 MHz real-time oscilloscope. The results are presented in Figs. 4(b)–4(d). Once the polarization in the cavity is properly aligned using the PC, the laser provides a very stable pulse train with a pulse repetition rate of 7.19 MHz (139 ns pulse period) [Fig. 4(b)], confirmed from the ESA. Due to the limited bandwidth of the real-time oscilloscope and the unavailability of a 2 μm autocorrelator, the pulse duration could not be evaluated at this time. However, the absence of Kelly sidebands on the optical spectrum [Fig. 4(d)] could indicate that the laser does not provide transform-limited pulses. The large spectral bandwidth (30 nm FWHM) of the laser emission could indicate a noisy-pulse mode-locking regime, caused by large negative value of net cavity dispersion [8].

In conclusion, we have experimentally determined the nonlinear coefficient γ and the anomalous group velocity dispersion (GVD) β_2 of a core-pumped TDF by degenerate FWM at 2 μm. Small core diameter and Al_2O_3 – La_2O_3 core doping result in values in the range 3.6–4.1 $W^{-1} \cdot km^{-1}$ for γ. Studies of SiO_2 fibers with La_2O_3 doping have demonstrated a significant rise of the nonlinear index n_2 (5.8 10^{-20} m^2 W^{-1} for 10.5 mol. % of lanthanum oxide) [18]. In case of TmDF200 fiber, the manufacturer does not disclose the material composition, therefore a theoretical evaluation of n_2 is not possible. Independent linear dispersion measurements using an all-fiber MZI confirm the GVD of about −20 ps^2/km. Moreover, no resonant dispersion changes were observed when a 1.6 μm pumping was applied to the TDF (conversely to EDFs). Such characteristics make core-pumped TDFs attractive for mode-locked fiber laser applications. As demonstrated, a NPR-based MLL can be built involving nonlinear polarization evolution directly in the doped fiber.

Funding. Swiss National Science Foundation (SNSF) (200021_140816); European Research Council (ERC) (2012-StG 306630-MATISSE).

Acknowledgment. We thank the Laboratoire de Physique des Lasers, Atomes et Molécules, Lille University of Science and Technology (France) for the fabrication of 2000 and 2008 nm FBGs. We would like to acknowledge fruitful discussions with Dr. Armand Vedadi.

REFERENCES

1. S. Ishii, K. Mizutani, H. Fukuoka, T. Ishikawa, B. Philippe, H. Iwai, T. Aoki, T. Itabe, A. Sato, and K. Asai, Appl. Opt. **49**, 1809 (2010).
2. R. J. De Young and N. P. Barnes, Appl. Opt. **49**, 562 (2010).
3. D.-C. Hong, W. Jia, H. Yu, L.-L. Ren, J.-L. Hao, G. Liang, T. Zhuang, Y.-H. Chun, L. Xiang, J.-Y. Hong, D. Qiang, and W. Qiang, Sci. Rep. **5**, 14542 (2015).
4. S. D. Jackson, Nat. Photonics **6**, 423 (2012).
5. M. N. Petrovich, F. Poletti, J. P. Wooler, A. M. Heidt, N. K. Baddela, Z. Li, D. R. Gray, R. Slavik, F. Parmigiani, N. V. Wheeler, J. R. Hayes, E. Numkam, L. Grüner-Nielsen, B. Pálsdóttir, R. Phelan, B. Kelly, J. O'Carroll, M. Becker, N. MacSuibhne, J. Zhao, F. C. G. Gunning, A. D. Ellis, P. Petropoulos, S. U. Alam, and D. J. Richardson, Opt. Express **21**, 28559 (2013).
6. H. Li, J. Liu, Z. Cheng, J. Xu, F. Tan, and P. Wang, Opt. Express **23**, 6292 (2015).
7. G. Sobon, J. Sotor, I. Pasternak, A. Krajewska, W. Strupinski, and K. M. Abramski, Opt. Express **21**, 12797 (2013).
8. J. Li, Z. Zhang, Z. Sun, H. Luo, Y. Liu, Z. Yan, C. Mou, L. Zhang, and S. K. Turitsyn, Opt. Express **22**, 7875 (2014).
9. M. A. Chernysheva, A. A. Krylov, N. R. Arutyunyan, A. S. Pozharov, E. D. Obraztsova, and E. M. Dianov, IEEE J. Sel. Top. Quantum Electron. **20**, 448 (2014).
10. L. E. Nelson, E. P. Ippen, and H. A. Haus, Appl. Phys. Lett. **67**, 19 (1995).
11. A. M. Heidt and D. J. Richardson, IEEE J. Sel. Top. Quantum Electron. **20**, 525 (2014).
12. Z. Li, S. U. Alam, Y. Jung, A. M. Heidt, and D. J. Richardson, Opt. Lett. **38**, 4739 (2013).
13. S. Kharitonov, A. Billat, L. Zulliger, S. Cordette, A. Vedadi, and C.-S. Brès, in *Conference on Lasers and Electro-Optics* (2015), paper JTu5A.31.
14. M. E. Marhic, *Fiber Optical Parametric Amplifiers, Oscillators and Related Devices* (Cambridge University, 2007).
15. S. D. Agger and J. H. Povlsen, Opt. Express **14**, 50 (2006).
16. H.-T. Shang, Electron. Lett. **17**, 603 (1981).
17. R. K. Hickernell, K. Takada, M. Yamada, M. Shimizu, and M. Horiguchi, Opt. Lett. **18**, 19 (1993).
18. C. Karras, D. Litzkendorf, S. Grimm, K. Schuster, W. Paa, and H. Stafast, Opt. Mater. Express **4**, 2066 (2014).